

## **Experimental Investigation and Nonlinear Analysis of Hybrid Reinforced Concrete Deep Beams**

**Prof. Dr. Ammar Yaser Ali**

**Mrs. Maha Ghazi Zghair**

**Babylon University, Engineering College, Civil Department**

**Received 16 March 2015**

**Accepted 7 May 2015**

### **ABSTRACT**

This study presents experimental and theoretical investigation of the overall shear behavior of reinforced concrete deep beams made from hybrid concrete strength : Normal strength concrete (NSC) in tension zone and high strength concrete (HSC) in compression zone. The experimental work included testing of nine models of hybrid reinforced concrete deep beams under the effect of two point loads. One of the beams was tested as pilot and the other eight beams were divided into two groups namely group (A) and group (B) to study the effects of the following parameters: (HSC) the layer thickness, the effect of presence of web reinforcement and method of casting (i.e. monolithically or at different times), on the ultimate shear strength, the cracking load, the cracking pattern, the deflection, the ductility and failure modes.

The experimental test results obtained from the adopted hybridization technique of (HSC) and (NSC) have shown that for beams made from (HSC) (about 45MPa) with a layer in compression zone of thickness (25 - 50)% of total beam depth, the ultimate shear strength was increased about (11.2 - 19.5)% for beams without web reinforcement and (16.75 - 22.25)% for beams with minimum web reinforcement. It has also shown that, the first cracking load was increased about (32.8 - 48)% and (43.4 - 57.9)% for beams without and with web reinforcement, respectively.

The hybrid concrete beams that cast monolithically, have exhibited an increase in ductility about (13.3- 22.6) % and (17.3 - 26.3) % for specimens without and with web reinforcement, respectively. While, the hybrid concrete beams with construction joint and epoxy resin layer of thickness about (1mm), have exhibited larger increasing in ductility about (28.7%) and (30.2%) for specimens without and with web reinforcement, respectively.

On the other hand, a non-linear three dimensional finite elements simulation using *ANSYS* computer program was adopted to trace the load-deflection response, cracking pattern and ultimate shear strength of the tested reinforced hybrid concrete beams with or without construction joint. Afterward, a parametric study has been conducted to investigate the effects of many important variables (compression strength for (HSC) layer, thickness of (HSC) layer, shear span to effective depth ratio ( $\frac{a}{d}$ ), thickness of resin bond layer).

Comparison between the analytical and experimental results has shown a reasonable agreement of the load-deflection response, where, the average of the maximum difference in first cracking and ultimate loads was (13)% and (9.6)%, respectively.

## التقصي العملي والتحليل اللاخطي للأعتاب الخرسانية المسلحة العميقة الهجينة

## الخلاصة

تقدم هذه الدراسة بحثاً نظرياً وعملياً لسلوك القص العام في العتبات الخرسانية المسلحة العميقة المصنوعة من الخرسانة الهجينة: الخرسانة عادية المقاومة (NSC) في منطقة الشد والخرسانة عالية المقاومة (HSC) في منطقة الضغط. تضمن الجزء العملي فحص تسعة موديلات من الأعتاب الخرسانية المسلحة العميقة الهجينة تحت تأثير فحص نقطي ثنائي التحميل. أحد هذه العتبات فحصت كعتبة إرشادية والعتبات الثمانية الأخرى قسمت إلى مجموعتين (A و B) لدراسة تأثيرات: سمك طبقة الخرسانة عالية المقاومة (HSC) , وجود حديد تسليح الوتر (web) وطريقة الصب مباشرة أو في أوقات مختلفة (أي وجود مفصل إنشائي أفقي) على مقاومة القص العظمى, حمل التشقق, نمط التشقق, الهطول, المطاوعة (المطيلية) وأنماط الفشل.

نتائج البرنامج العملي المستحصلة من تقنية التهجين المثبتة للخرسانة العادية والعالية المقاومة بينت إن العتبات المصنوعة من الخرسانة العالية المقاومة (45 MPa) في منطقة الضغط بسمك (25-50)% من عمق العتبة الكلي مقاومة القص العظمى لها زادت بنسبة حوالي (11.2-19.5)% للعتبات بدون تسليح الوتر و (16.75-22.25)% للعتبات ذات تسليح الوتر, على التوالي. كذلك حمل التشقق الأول زاد بنسبة حوالي (32.8-48)% و (43.4-57.9)% للعتبات بدون ومع تسليح الوتر, على التوالي.

العتبات الهجينة المفحوصة (المصوبية بشكل مباشر) أبدت زيادة في المطاوعة (المطيلية) بنسبة حوالي (13.3-22.6)% و (17.3-26.3)% للعتبات بدون ومع تسليح الوتر, على التوالي. بينما العتبات الهجينة ذات المفصل الإنشائي مع وجود طبقة من مادة الأبيوكسي بسمك حوالي 1 ملم) أبدت زيادة أكبر في المطاوعة بنسبة حوالي (28.7)% و (30.2)% للعتبات بدون ومع تسليح الوتر, على التوالي.

في الجزء التحليلي, تم استخدام عناصر محددة ثلاثية الأبعاد لاخطية في برنامج العناصر المحددة (ANSYS) لتقصي تصرف منحنى الحمل-الهطول, نمط التشقق و مقاومة القص العظمى للعتبات الخرسانية المسلحة العميقة الهجينة مع أو بدون وجود مفصل إنشائي بالإضافة إلى دراسة تأثير متغيرات مهمة عديدة. المقارنة بين النتائج العملية والتحليلية أبدت توافقاً معقولاً في منحنى الحمل-الهطول, حيث كان الفارق الأعظم في حمل التشقق الأول والحمل الأقصى ذو نسبة حوالي (13)% و (9,6)%, على التوالي.

## 1. Introduction

Deep beams are structural elements loaded as beams but having small shear span to depth ratio. A deep beam in general, has a depth much greater than the normal, while the thickness in the perpendicular direction is much smaller than either span or depth.

(ACI-code 318R-08) defines deep beams as those, which have clear span to overall depth ratio less than four ( $l_n/h \leq 4$ ), or the shear span to effective depth ratio less than two ( $a/d \leq 2$ ), and should be loaded on one face and supported on the opposite face, so that the compression struts can develop between the loads and supports. Reinforced concrete deep beams are widely used in many structural engineering applications, such as: transfer girders, pile caps, offshore structures, shear walls, wall footing, floor diaphragms and complex foundation system (ASCE committee 426).

Utilization of high strength concrete in construction sector has increased due to its improved mechanical properties compared to ordinary concrete. One such mechanical property, shear resistance of concrete beams is an intensive area of research (Sudheer et al., 2011). The relatively recent development in concrete technology has led to produce high compressive strength concrete of (40 to 150 MPa). High strength concrete can be produced by adding high range water-reducing admixtures (Superplasticizer) and/or other admixtures (silica fume or fly ash) to Portland cement concrete (Newman and Choo, 2003).

Although high strength concrete offers advantages in terms of performance and economy of construction, the brittle behavior of the material remains a major drawback in some structural applications especially in earthquake resistant structures. Since strength and ductility of concrete are inversely proportional, high strength concrete is significantly more brittle than the normal strength concrete (Ashour and Wafa, 1993). In order to overcome the problems in terms of

deformability and ductility of concrete beams reinforced with steel bars, alternative solutions of using hybrid concrete concept is presented in this study.

## **2. Objective of Research**

This work is intended to introduce experimental investigation of the ultimate shear strength, cracking patterns, modes of failure, deflection and ductility of hybrid reinforced concrete deep beams composited of HSC in compression zone and NSC in tension zone. The two types of concrete will be either cast monolithically (at same time) or cast with horizontal construction joint (at different times). The effects of high strength concrete layer, web reinforcement and construction joints on overall shear behavior will be studied.

Evaluate the validity and accuracy to carry out finite element model to analyze the nonlinear behavior of reinforced hybrid concrete deep beam up to failure by using *ANSYS* computer program. As well as, parametric study of many important variables, such as: compressive strength of (HSC) layer, depth of (HSC) layer, shear span to effective depth ratio and thickness of resin bond layer.

## **3. Description of Specimens**

The experimental study consists of examining the use of two test groups (A and B). All beams are designed to fail in shear prior to flexure according to (*ACI-318Code*) specifications. Group (A) had no web reinforcement, while Group (B) included web reinforcement. The two test groups (A and B) are made of two different concrete mixes which are (25 and 45) MPa with normal and high strength concrete at tension and compression zones, respectively. For the two groups, eight models of deep beams are tested and the main parameters were identified to be: thickness of HSC layer in compression zone (25 and 50) % of total depth, shear reinforcement ratio (0.0 and 0.5)% and presence of construction joint. The type of concrete at tension zone and longitudinal reinforcement ratio are kept constants. Designation and details of all test beams are reported and presented in **Table (1)**.

Test specimens having a total length ( $l=1400\text{mm}$ ), span length ( $l_n=1200\text{mm}$ ), overall depth ( $h=450\text{mm}$ ), effective depth ( $d=400\text{mm}$ ) and width ( $b=100\text{mm}$ ) with shear span to effective depth ratio ( $a/d$ ) about 1.0 to ensure that tied-arch action of deep beam would be developed.

Four ( $\varnothing 12\text{mm}$ ) diameter of deformed bars were provided as longitudinal tension reinforcement with ( $\rho$  about 1.13%) and ( $2\varnothing 10\text{mm}$ ) to be used as compressive bars. The vertical and horizontal shear reinforcement were omitted from the beams of group (A) to emphasize the effect of high strength concrete layer without stirrups on shear capacity of hybrid deep beam, while the beams of group (B) minimum vertical and horizontal web reinforcement ( $\varnothing 4\text{mm} @ 100 \text{ mm c/c}$ ) with shear reinforcement ratio about (0.5%) were used to study their effect on shear capacity for hybrid beam, *as shown in Figure (1)*.

## **Material Properties**

The cement used in casting all the specimens was Ordinary Portland cement Company commercially known (**TASLUJA-JESSER**). Also, natural sand from (**WLAIT-ALI**) region was used as a fine aggregate. The fine aggregate was sieved at sieve size (2.36mm) to separate the aggregate particle of diameter greater than 2.36mm. Locally available gravel of 19 mm maximum size was used. Clean tap water was used for casting and curing of all the specimens. Normal strength concrete was used to cast all specimens with different percentage of cross-section depth. It was decided to choose a mix of 1:1.41:2.64 (by weight) cement, sand, gravel, respectively and 0.41 water cement ratio. The compressive strength of NSC was about 25 MPa at age of (28 days). The employed chemical admixtures (Superplasticizer), low water-cement ratio and high cement content make the design of high strength concrete a highly critical process than the design of

normal strength mixtures. Therefore, several trial mixes have been made through the earlier stage of the present work. The high strength concrete mix is given a compressive strength of about (45MPa) at age (28 days).

The yield strength of steel ( $f_y$ ) for bar size (12, 10, 4 mm) was (643, 596, 568 MPa) respectively with the value of modulus of elasticity  $E_s$  was taken as (200 GPa) for all sizes. The mechanical properties of the Superplasticizer (*Glenium 54*) and Epoxy resin (*CONCRETSIVE 1414*) sheet are given in **Table (2)** according to manufacturing specifications of BASF Company, Dubai.

#### **4. Test Setup**

The hydraulic universal testing machine was used to test the beam specimens as well as the control specimens. The testing machine has a capacity of (2000 kN) available in the Structural Laboratory in Civil Engineering Department, College of Engineering, Al-Qadissiya University, as shown in **Figure (2)**.

### **6. Experimental Results**

#### **6.1 Cracking Patterns**

In general, there are three stages of load-deflection response, these are: elastic-uncracked, elastic-cracked and ultimate stage, where the first stage terminates when the cracks develop. On the other hand, there are three types of developed cracks, flexural cracks, flexure-shear cracks and inclined (diagonal) shear cracks, as shown in **Figure (3)**.

**The Specimen A-1N** is made from normal strength concrete for overall depth and does not include web reinforcement (stirrups). The first visible cracks are narrow diagonal shear cracks in the shear-span region formed at a load of about (125kN). A few flexural cracks formed later at mid span region at a load of about (200kN). Then the collapse happened suddenly by splitting the beam into two pieces at load about (374kN).

**The Specimen B-1SN** is made from normal strength concrete for overall depth; it is similar to the specimen (A-1N) except including of web reinforcement (stirrups). Firstly, the formation of diagonal crack through shear span was started at a load of about (145kN). When the load reached about (208kN) the narrow flexural cracks appeared at constant moment region. As the load increased the diagonal cracks developed. Afterward, the failure occurred due to concrete crushing along strut direction at ultimate load about (400kN). It can be noticed that the specimen (B-1SN) has larger shear capacity when compared with the specimen(A-1N) by about(7%) and larger stiffness of post-cracking response and also lesser deflection at service load (65% from ultimate load) about (18.2%).

**The Specimens Cast Monolithically (A-2NH25, A-3NH50)** are made from two types of concrete, normal strength concrete (NSC) and high strength concrete (HSC) with (25% and 50%) of overall depth at compression zone, respectively. For specimens (A-2NH25 and A-3NH50), diagonal cracks formed initially at a load approximately of (166kN) and (185kN) (40% and 41.4% of peak load), respectively, and larger than the specimen (A-1N) by about (32.8% and 48%), respectively The increase in first cracking loads may arise from the increase in beam stiffness due to the increase in the ultimate compressive strength of compression zone. A flexural crack formed at a load about (208kN) for specimen A-2NH25 in a constant moment region, and remained a narrow width through the test, while in the specimen (A-3NH50) flexural cracks are not observed. Finally, the diagonal-splitting failure occurred at a load about (416 and 447kN) for specimens (A-2NH25 and A-3NH50) which are larger about (11.2% and 19.5%) with respect to control beam (A-1N), respectively, as shown in **Figure (3)** and **Table (3)**.

**The Specimen Cast with Construction Joint (A-4NH25E)** is made from (NSC) in tension zone and (HSC) in compression zone of thickness (25%) of total depth. The specimen is similar to the

specimen (A-2NH25) in all details, but the difference was existence of the construction joint with epoxy resin layer positioned between two layers of concrete to provide adequate bond between them. This case may be important during concrete structures maintenance, where the layers of new concrete are often applied to an old structure in order to repair and /or strengthen structural element. In general, the first visible cracks are inclined shear cracks at load about (145 kN) (36.7% of the ultimate load) and larger than the specimen (A-1N) by about (16%) due to increase in the ultimate compressive strength of compression concrete zone. Finally, the diagonal splitting failure is occurred prior to appearance of the flexural cracks at ultimate load about (395kN), which increased about (5.6%) with respect to control specimen (A-1N).

**The Specimens Cast Monolithically, (B-2SNH25, B-3SNH50)** are made from two types of concrete, (NSC) in tension zone and (HSC) at compression zone of thickness (25% and 50%) of total depth, respectively. These specimens are similar to the specimens (A-2NH25 and A-3NH50) in all details, but the difference is existence of minimum horizontal and vertical ( $\varnothing 4\text{mm} @ 100 \text{mm}^c/c$ ) shear reinforcement.

This model of hybridization for specimens (B-2SNH25 and B-3SNH50) have increased the first crack loads about (43.4% and 57.9% with respect to the control specimen B-1SN), respectively. The increase in first cracking loads may arise from the increase in beam stiffness due to the increase in the ultimate compressive strength of compression zone and existence of web reinforcement. When the loading level increased, the diagonal cracks developed and the concrete at strut direction and under loading plate is crushed at load about (467and 498kN) for specimens (B-2SNH25 and B-3SNH50), respectively.

The ultimate load for these specimens increased about (16.75% and 22.25%) with respect to the control specimen (B-1SN), respectively, as listed in **Table (3)**.

**The Specimen Cast with Construction Joint (B-4SNH25E)** was cast in two stages with interval carnal (28 days). First, the normal strength concrete (NSC) part was cast at bottom tension zone and after its final hardening, the high strength concrete (HSC) layer was cast later at compression zone (25% of total depth) after the epoxy layer was put to provide adequate bond between two different concrete layers.

The first visible crack is inclined shear crack a long strut direction at load about (166kN) (37% of the ultimate load). On the other hand, the first cracking load of this specimen increased about (14.5% of control beam B-1SN) due to the increase in moment of inertia of gross section, while it decreased about approximately (20.2% of similar specimen B-2SNH25) due to the presence of the construction joint which reduced the stiffness of the beam, and then reduced the cracking load.

As the load increasing, the diagonal cracks developed and widened rapidly toward supporting and loading points, and then the diagonal strut compression failure and crushing of concrete occurred along line that join support and point load at load about (447kN), as shown in **Figure (3)**.

## **6.2 Load-Deflection Curves**

All the beams of this study were designed to fail in shear according to (*ACI-318Code*) because the mechanical behavior and design of deep beams are governed by shear and its load carrying capacity depends on the strength of compressive strut that join the loading and reaction points (Tied-Arch Action).

In general, there are three stages of load-deflection response, these are: elastic-uncracked, elastic-cracked and ultimate stage, where the first stage terminates when the cracks develop. In elastic-uncracked stage, deflection increase linearly in all beams with loading since the materials in compression and tension zone are in elastic manner. In elastic-cracked (post-cracking) stage there is also linear relationship between load and deflection but with reduction in slope. After this stage, the slope decrease largely and aggravated increments in deflection with small increase in loading level up to failure. Load – deflection curves for two groups are shown in **Figure (4)**.

### **6.3 Ductility**

Ductility can be defined as the ability to sustain inelastic deformations without losing of the load carrying capacity prior to failure. In the present study, the experimental ductility ratios are calculated according to the deflection at ultimate load divided by the deflection at yielding (**Winter and Nilson, 1978**). **Table (4)** illustrates the ductility ratio  $\mu$  of the tested beams.

For specimens of series A, (A-2NH25, A-3NH50 and A-4NH25E) which had high strength concrete in compression zone (25%, 50% and 25% with construction joint) of total depth, respectively, the ductility was increased (13.3% , 22.6% and 28.7%), respectively, in comparison with control beam (A-1N), while the specimens of series B, (B-2SNH25, B-3SNH50 and B-4SNH25E), had high strength concrete in compression zone (25%, 50% and 25% with construction joint) of total depth, respectively, the ductility was increased (17.3%, 26.3% and 30.2%), respectively in comparison with control beam (B-1SN).

The increase in the ductility can be attributed to the slight increase in ultimate load capacity, which produces higher ultimate deflection, and also due to the presence of construction joint between two types of concrete, which decreased the beam stiffness, and then increased the ultimate deflection.

## **7. Numerical Analysis**

The aim of this section is to compare between the finite element model results and the experimental results to verify the adequacy of elements type, material modeling, and convergence criteria to model the response of the reinforced hybrid concrete deep beams, which consist of different types of concrete (NSC and HSC), with or without web reinforcement and with or without construction joints.

This section includes the analysis of the tested beams and parametric study of many variables by using a powerful nonlinear finite element method package ANSYS software (version 12.0).

### **7.1 Description of Specimens in Finite Element**

By taking advantage of the symmetry for both beam's geometry and loadings, a quarter of the beam was used for finite element analysis, as shown in **Figure (5)**.

An important step in finite element modeling is the selection of the mesh density. A convergence of results is obtained when an adequate number of elements are used in a model. This is practically achieved when an increase in the mesh density has a negligible effect on the results. Therefore, in this finite element modeling, a convergence study is carried out to determine an appropriate mesh density. Three types of mesh are used to find the best mesh size for control beam (A-1N) and hybrid beam (A-2NH25).

**Figure (6)** shows the relationship between the number of elements and mid-span deflection. It can be observed from the figure below that the difference can be neglected when the number of elements increased from (1138) to (4182) for the control deep beam, from (1194) to (4294) for the hybrid beam; therefore, the (1138 and 1194) models select for model the A-1N and A-2NH25, respectively.

### **7.2 Modeling of Reinforced Concrete Control Beam**

In the finite element model, a solid element (Solid 45) was used to model the steel plates at the support and loading point. In addition, (Solid 65) was used to model the two types of concrete. Node to node contact elements were used to model construction joints between two types of concrete old pre-cast (NSC) and new cast-in-place (HSC), as shown in **Figure (7)**. Link-8 element was employed to represent the steel reinforcement for group (A) and (B), as shown in **Figure (8)**. In this study, a perfect bond between concrete and steel reinforcement is assumed.

Boundary conditions need to apply at points of symmetry and where the supports and loads exist. To model the symmetry, nodes on these planes must be constrained in the perpendicular directions. Therefore, the nodes in  $U_x$  and  $U_z$  have a degree of freedom equal to zero for plane of mid-span and plane of longitudinal, respectively, as shown in **Figure (9)**. The support was modeled in such a way as a roller. A single line of nodes on the plate is given constraint in the  $U_y$  direction. By doing this, the beam will be allowed to rotate at the support.

The external distributed applied load was represented by dividing the total distributed load on the top nodes according to area rounded of each node to represent the distributed load in ANSYS program. **Figure (10)** shows the details of applied load at loading plate.

### **7.3 Results of Finite Element Analysis**

All tested beams will be analyzed by using ANSYS computer program, as mentioned previously. This comparison includes: first cracking load, cracking patterns, ultimate load and deflections at service and ultimate load.

#### **7.3.1 First Cracking Loads**

The comparison between experimental and numerical results of the first cracking load is shown in **Table (5)**.

**Table (5)** shows a reasonable agreement in the comparison between the experimental cracking loads of the beams,  $P_{cr(EXP.)}$ , and the numerical cracking loads from the finite element models,  $P_{cr(FEM)}$ . The first cracking load obtained from numerical data showed results lower than the experimental data recorded with difference about (13%) as an average.

#### **7.3.2 Load-Deflection Response**

Deflections (vertical displacements) were measured at mid-span at the center of the bottom face of the beams. The load versus deflection plots for all beams obtained from the numerical study together with the experimental plots are presented and compared in **Figure (11)**.

A relatively stiffer numerical response has been observed at the advanced stages of loading. As a general response, the load deflection plots for the beams from the finite element analysis gave an acceptable agreement when compared with the experimental data, where the three stages of load-deflection response (elastic-uncracked, elastic-cracked and elasto-plastic) can be noticed.

#### **7.3.3 Ultimate Shear Strength**

**Table (6)** shows the comparison between the ultimate loads of the experimental (tested) beams and the numerical models from finite element analysis. It is clear that the loads obtained from numerical simulation gave acceptable convergence with the corresponding values of the experimental test beams with different (9.6%), as shown in the table below.

#### **7.3.4 Ultimate and Service Mid-Span Deflections**

A comparison between mid-span deflections at ultimate and service load of the experimental tested beams with numerical mid-span deflection from finite element models, where the service load equal (0.65×ultimate load) (**Kheder et al., 2010**), is shown in **Table (7)**.

As shown in **Table (7)**, in comparison with the experimental values, the numerical models showed increasing in ultimate deflections for the all beams about (18.7%) as an average, while the

deflections at service load are lower than the experimental data recorded with difference about (9.8%) as an average.

#### **7.4 Parametric Study**

The effect of some selected parameters on overall shear behavior of homogenous and hybrid cross section deep beams are decided herein, as follows:

- 1- Compressive strength for high strength concrete (HSC) layer.
- 2- Thickness of high strength concrete (HSC) layer.
- 3- Shear span to effective depth ratio ( $\frac{a}{d}$ ).
- 4- Thickness of resin bond layer.

##### **7.4.1 Effect of Compressive Strength for High Strength Concrete (HSC) Layer**

To show the effect of compressive strength of high strength concrete layer, two cases (a, b) were studied. When the strength of high strength concrete layer increased from (25-200) MPa, the ultimate capacity increased largely about (21.8 - 66, 30.5 -80, 24.7 - 77.8, 35 - 83) % for the specimens (A-2NH25, B-2SNH25, A-3NH50 and B-3SNH50), respectively with higher stiffness and ultimate deflection, as shown in **Figure (12)**.

##### **7.4.2 Effect of Thickness for High Strength Concrete (HSC) Layer**

To explain the effect of thickness for HSC layer, two groups (A and B) were studied with varied of HSC depth to (25%, 50%, 75%, and 100 %) of total specimen depth. In general, when the HSC layer thickness increased causing increment in the beam stiffness and then led to failure at high level of ultimate load with slight increasing of mid-span deflection, as shown in **Figure (13)**.

##### **7.4.3 Effect of the Shear Span to Effective Depth Ratio ( $\frac{a}{d}$ )**

To show the effect of the shear span to effective depth ratio ( $\frac{a}{d}$ ), four specimens (A-2NH25, A-3NH50, B-2SNH25 and B-3SNH50) were studied with varied ( $\frac{a}{d}$ ) to (0.5, 0.75, 1, 1.25) for each specimen, as shown in **Figure (14)** and **Table (8)**.

##### **7.4.4 Effect of Resin Bond Layer**

To explain the effect of thickness of epoxy resin layer, two specimens (A-4NH25E and B-4SNH25E) were studied changing the epoxy resin thickness to (1, 2 and 3) mm. In general, when the gap between two types of concrete of these specimens that was full of the epoxy resin increased to (1, 2 and 3)mm, the ultimate load decreased about (5 - 27.7)% and (3 - 20.9)% for specimens (A-4NH25E) and (B-4SNH25E), respectively with increasing in service mid-span deflection, as shown in **Figure (15)**.

## **8. Conclusions**

### **8.1 Conclusions for Experimental Work**

- 1- Presence of high strength concrete (HSC) layer in compression zone with thickness (25 and 50)% of total depth led to increase the ultimate shear strength by about (11.2 and 19.5)% for specimens without web reinforcement (group A) and about (16.75 and 22.25)% for specimens with minimum web reinforcement (group B), respectively.
- 2- The first cracking loads were increased by about (32.8 - 48) % for specimens of (group A) and about (43.4 - 57.9)% for specimens of (group B) due to hybridization technique.
- 3- Presence of construction joint in hybrid sections produced slight reduction in ultimate shear strength about (5 and 4.3) % for specimens without and with web reinforcement, respectively, when compared with hybrid sections cast (monolithically). This means that the casting technique (wet-on-wet) is favorable.
- 4- The tested hybrid beams with (HSC) layer that had no web reinforcement exhibited an increase in ductility between (13.3% - 22.6%), while the tested beams that had minimum web reinforcement exhibited larger increasing in ductility between (17.3% - 26.3%).
- 5- Presence of construction joint with epoxy resin layer of thickness about (1mm) caused increasing in ductility about (28.7%) for specimen without web reinforcement and about (30.2%) for specimen with web reinforcement.
- 6- For hybrid deep beams of (NSC) and (HSC) without web reinforcement, the mode of failure was splitting. While the hybrid deep beams with minimum web reinforcement, the mode of failure altered from splitting to crushing or compression of strut.

### **8.2 Conclusions for Finite Element Analysis**

- 1- The general behavior of the finite element models represented by the load-deflection plots at mid-span showed acceptable agreement with results of experimentally tested beams, where the deflections at service load were lower than the experimental data recorded with difference about (9.8%) as average.
- 2- The ultimate shear loads predicted by the numerical analysis were close to that measured during experimental testing with maximum difference (9.6%) as average.
- 3- The first cracking load obtained from numerical data showed results lower than the experimental data recorded with difference about (13%) as average.
- 4- The ultimate shear strength for hybrid reinforced concrete deep beams increased about (21.8-77.8 and 30.5-83) MPa for specimens of group A and B when the compressive strength of (HSC) layer increased from (25-200) MPa, respectively, with higher stiffness and ultimate deflection.
- 5- When the thickness of HSC layer increased to (25, 50, 75, 100)% of total depth, the ultimate load increased about (12.8, 18.6, 49.5, 73.4) % for group (A), while it increased about (16.6, 24, 71.3, 97.2)% for group (B), respectively.

- 6- The specimens with full (HSC) section have more ultimate shear strength than hybrid section but less ductility.
- 7- The ultimate load decreased about (6.3-19.6)%, when the shear span to effective depth ratio ( $\frac{a}{d}$ ) increased about (0.5-1.25) of the tested beams but the service load deflection increased about (15.4-57.4)%.
- 8- The ultimate load decreased about (5-27.7) % and (3-20.9)% for specimens(A-4NH25E)and(B-4SNH25E),respectively with increasing in service mid-span deflection when the epoxy resin thickness changed to (1, 2 and 3) mm.

## References

- [1] ACI-ASCE Committee 426, "*Shear Strength of Reinforced Concrete Members* ", Proceedings, ASCE 1973; 99(6), PP. 1091-1187.
- [2] Ansys, "*ANSYS Help*", Release 9.0, copyright 2004.
- [3] Ashour, S.A., and Wafa, F.F., "*Flexural Behavior of High Strength Fiber Reinforced Concrete Beams*", ACI Structural Journal, Vol. 90, No. 3,May-June 1993, pp. 279-287.
- [4] Concrevice, "*CONCREVICE® 1414 Epoxy Bonding Agent for Concrete Repairs, Bonding Concrete to Concrete, Steel and Granolithic Toppings*", Technical Data Sheet, Edition 2, 2006.
- [5] Glenium, "*GLENIUM®54 A high Performance Concrete Superplasticiser Based on Modified Polycarboxylic Ether*", Technical Data Sheet, Edition 2, 2010.
- [6] Newman, J., and Choo, B.S., "*Advanced Concrete Technology*", 1<sup>st</sup>Edition,Elsevier Ltd., UK 2003, (616) p.

**Table (1):** Designation and Details of test beams

<b>Group</b>	<b>Beam No.</b>	<b>Beam Designation</b>	<b>Depth of concrete</b>		<b>Construction joint *</b>
			<b>NSC (mm)</b>	<b>HSC (mm)</b>	
<b>(A)</b> <i>Hybrid Deep Beams without Web Reinforcement</i>	<i>A-1</i>	<i>A-1N</i>	450	-----	<i>without</i>
	<i>A-2</i>	<i>A-2NH25</i>	337.5	112.5	<i>Without</i>
	<i>A-3</i>	<i>A-3NH50</i>	225	225	<i>Without</i>
	<i>A-4</i>	<i>A-4NH25E</i>	337.5	112.5	<i>with</i>
<b>(B)</b> <i>Hybrid Deep Beams with Web Reinforcement</i>	<i>B-1</i>	<i>B-1SN</i>	450	-----	<i>Without</i>
	<i>B-2</i>	<i>B-2SNH25</i>	337.5	112.5	<i>Without</i>
	<i>B-3</i>	<i>B-3SNH50</i>	225	225	<i>Without</i>
	<i>B-4</i>	<i>B-4SNH25E</i>	337.5	112.5	<i>with</i>

\* *without*: casting of (HSC) and (NSC) layers at same time (monolithically).

*With*: casting of (HSC) and (NSC) layers at different time.

Where each symbol in Table (1) refers to:

**A, B**: Group symbol, **1-4**: sequence of specimen in its group, **N**: Normal strength concrete, **H**: High strength concrete, **25, 50**: thickness of high strength concrete layer 25%, 50% of total depth, **E**:Epoxy resin existence between two types of concrete, **S**: Existence of web reinforcement (**Stirrups**).

**Table (2):** Properties of Superplasticizer and Epoxy Resin.

<b>Commercial name</b>	<b>Glenium 54</b>
<i>Chemical composition</i>	<i>Sulphonated melamine and naphthalene formaldehyde condensates</i>
<i>Subsidiary effect</i>	<i>Increased early and ultimate compressive strength concrete with minimal voids and optimum density</i>
<i>Form</i>	<i>Whitish to straw coloured liquid</i>
<i>Relative density</i>	1.07
<i>pH</i>	5-8
<i>Chlorides</i>	<i>Free from chlorides</i>
<b>Properties</b>	<b>CONCRETSIVE®1414</b>
<i>Mixed density @ 25°C</i>	1485kg/m <sup>3</sup>
<i>Pot life</i>	25°C 2 hours 40°C ¾ hours
<i>Tack free time</i>	25°C 9 hours 40°C 5 hours
<i>Full cure</i>	7 days

**Table (3):** Cracking Load, Ultimate Load and Failure Modes of the Tested Beams.

Beam symbol	Cracking Load, P <sub>cr</sub> (kN)		$\frac{P_{cr(i)} - P_{cr(r)}}{P_{cr(r)}} \times 100\%$	Ultimate Load, P <sub>u</sub> (kN)	$\frac{P_{u(i)} - P_{u(r)}}{P_{u(r)}} \times 100\%$	Mode of Failure
	Shear crack	Flexure crack				
A-1N	125	200	-----	374	-----	Diagonal splitting
A-2NH25	166	208	32.8	416	11.2	Diagonal splitting
A-3NH50	185	-----	48	447	19.5	Diagonal splitting
A-4NH25E	145	-----	16	395	5.6	Diagonal splitting
B-1SN	145	208	-----	400	-----	Strut crushing
B-2SNH25	208	239	43.4	467	16.75	Strut crushing
B-3SNH50	229	225	57.9	498	22.25	Strut crushing
B-4SNH25E	166	218	14.5	447	11.75	Diagonal compression

*i* :- Considered beam , *r*:- Reference beam

**Table (4):** Ductility Ratio of Tested Beams.

Beam symbol	Yielding deflection, Δ <sub>y</sub> (mm)	Ultimate deflection, Δ <sub>u</sub> (mm)	Ductility ratio, μ ( $\frac{\Delta_u}{\Delta_y}$ )	$\frac{\mu_i - \mu_r}{\mu_r} * 100\% (*)$
A-1N	3.5	5.25	1.5	-----
A-2NH25	4.1	7	1.7	13.3
A-3NH50	4.2	7.75	1.84	22.6
A-4NH25E	3.85	7.45	1.93	28.7
B-1SN	2.8	5	1.79	-----
B-2SNH25	3	6.3	2.1	17.3
B-3SNH50	3.2	7.25	2.26	26.3
B-4SNH25E	2.9	6.75	2.33	30.2

\* μ<sub>i</sub> = Ductility of considered beam

μ<sub>r</sub> = Ductility of reference beam

**Table (5):** Experimental and Numerical Results of First Cracking Loads

Beam No.	First Cracking Load (kN)				$\left(\frac{P_{Cr(FEM)}}{P_{Cr(EXP.)}}\right)_{(shear\ crack)}$
	Experimental $P_{Cr(EXP.)}$		Numerical $P_{Cr(FEM)}$		
	Shear Crack	Flexure Crack	Shear Crack	Flexure Crack	
A-1N	125	200	112	141	0.9
A-2NH25	166	208	143	150	0.86
A-3NH50	185	-----	154	176	0.83
A-4NH25E	145	-----	124	189	0.86
B-1SN	145	208	126	151	0.87
B-2SNH25	208	239	192	149	0.92
B-3SNH50	229	225	198	143	0.86
B-4SNH25E	166	218	149	144	0.9
The Average					0.87

**Table (6):** Comparison between Experimental, Finite Elements Ultimate Shear Loads.

Beam No.	Ultimate Shear Load (kN)		$\frac{(P_u)_{FEM}}{(P_u)_{EXP.}}$
	$(P_u)_{EXP.}$	$(P_u)_{FEM}$	
A-1N	374	414	1.106
A-2NH25	416	467	1.122
A-3NH50	447	491	1.098
A-4NH25E	395	446	1.129
B-1SN	400	439	1.097
B-2SNH25	467	512	1.096
B-3SNH50	498	544	1.092
B-4SNH25E	447	459	1.027
The Average			1.096

**Table (7):** Comparison between Experimental and Numerical Deflections at Service and Ultimate Loads.

Beam No.	Mid-span Deflection(mm)				$\frac{(\Delta s)_{FEM}}{(\Delta s)_{EXP.}}$	$\frac{(\Delta u)_{FEM}}{(\Delta u)_{EXP.}}$
	At Service Load		At Ultimate Load			
	$(\Delta s)_{EXP.}$	$(\Delta s)_{FEM}$	$(\Delta u)_{EXP.}$	$(\Delta u)_{FEM}$		
A-1N	2.5	2.15	5.25	6.75	0.86	1.286
A-2NH25	2.42	2.12	7	7.68	0.876	1.097
A-3NH50	2.3	1.95	7.75	9.2	0.848	1.187
A-4NH25E	3.2	3.15	7.45	8.84	0.984	1.186
B-1SN	2.2	2.1	5	5.82	0.954	1.164
B-2SNH25	2.12	2.05	6.3	7.54	0.967	1.197
B-3SNH50	2	1.65	7	8.69	0.825	1.241
B-4SNH25E	2.5	2.25	6.75	7.73	0.9	1.145
The Average					0.902	1.187

**Table (8):** Effect of Shear Span to Effective Depth Ratio ( $\frac{a}{d}$ ) on the Numerical Ultimate Load and Mid-Span Deflection at Service Load.

Beam No.	$a/d$	Numerical ultimate load(kN)	Numerical mid-span deflection at service load (mm)	Decrease Of ultimate load %	Increase of deflection at service load %
A-2NH25	0.5	543	1.62	-----	-----
	0.75	495	1.98	9	22.2
	1	467	2.12	14	30.8
	1.25	423	2.55	22	57.4
A-3NH50	0.5	565	1.51	-----	-----
	0.75	517	1.75	8.5	16
	1	491	1.95	13	29.1
	1.25	454	2.25	19.6	49
B-2SNH25	0.5	587	1.58	-----	-----
	0.75	545	1.88	7.2	19
	1	512	2.05	12.8	29.7
	1.25	496	2.45	15.5	55.1
B-3SNH50	0.5	618	1.3	-----	-----
	0.75	579	1.5	6.3	15.4
	1	544	1.65	11.9	26.9
	1.25	536	1.93	13.3	48.4

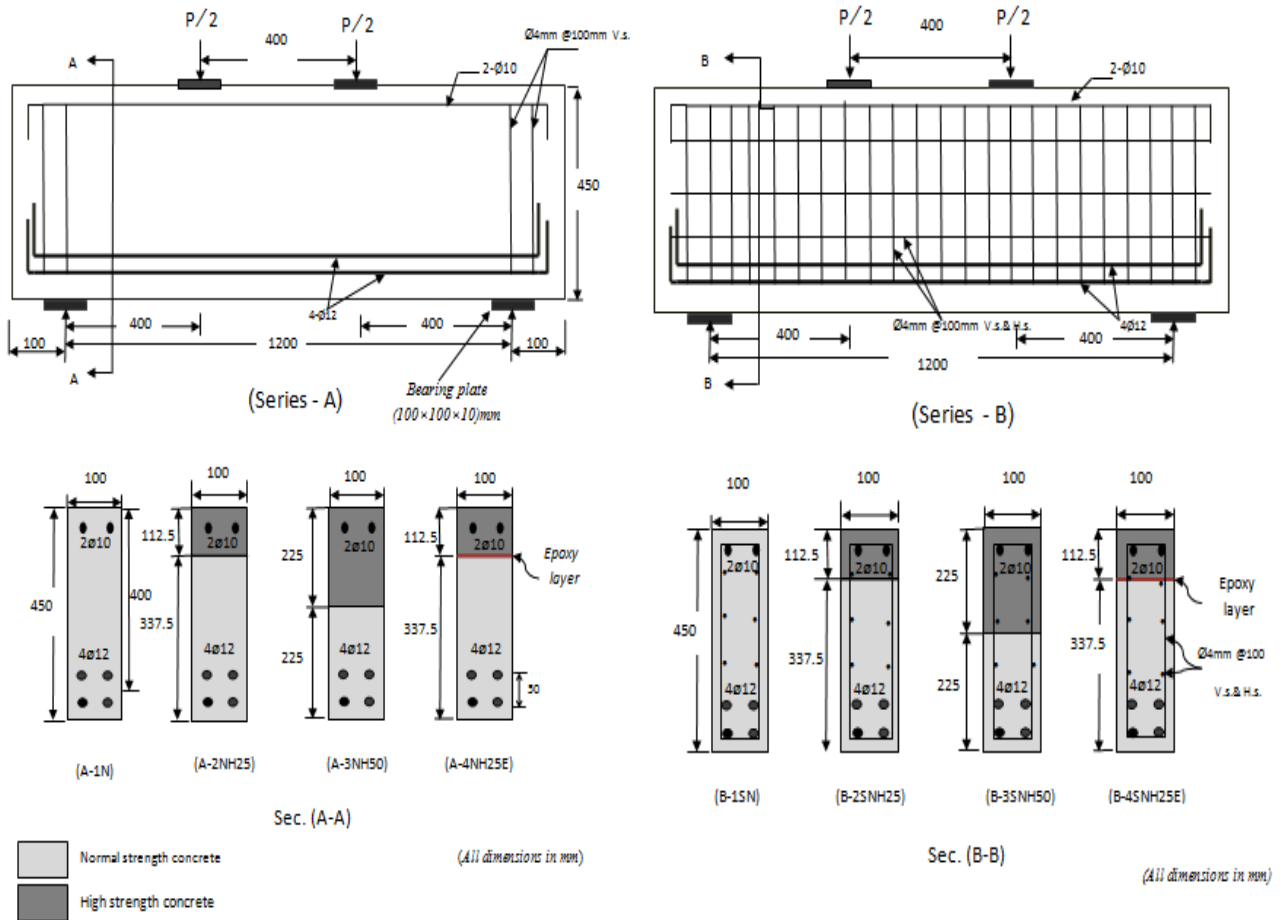


**Figure (1):** Loading and Specimens Details;

(a) Series A (without web reinforcement)

(b) Series B (with web reinforcement)



**Figure (2):** Testing Machine Used in This Work.

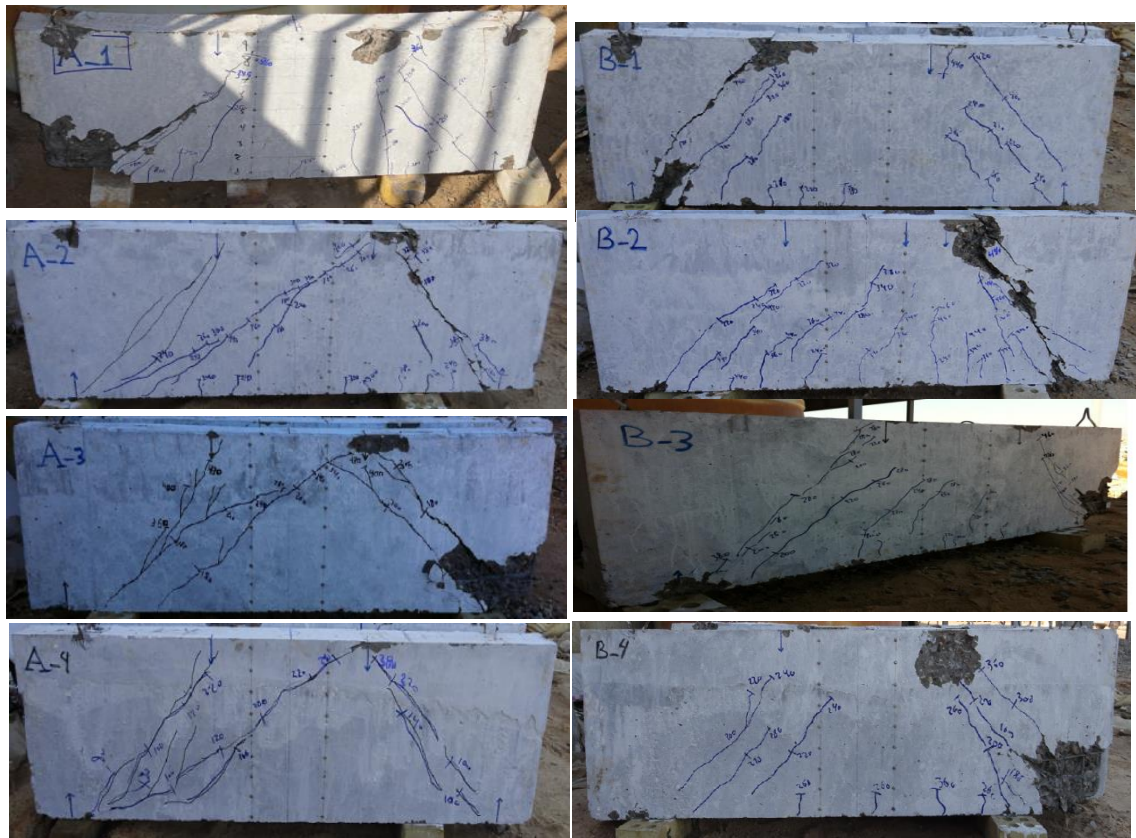


Figure (3): Crack Patterns of all Specimens.

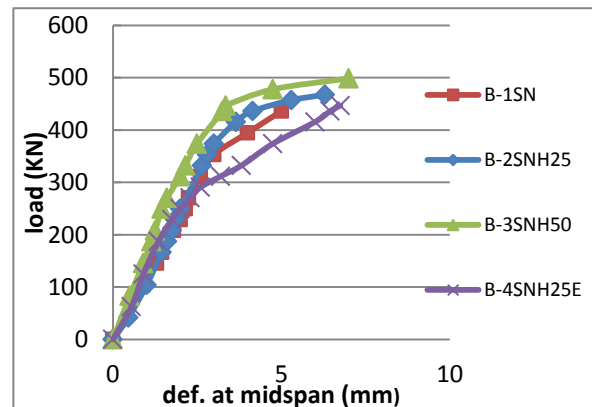
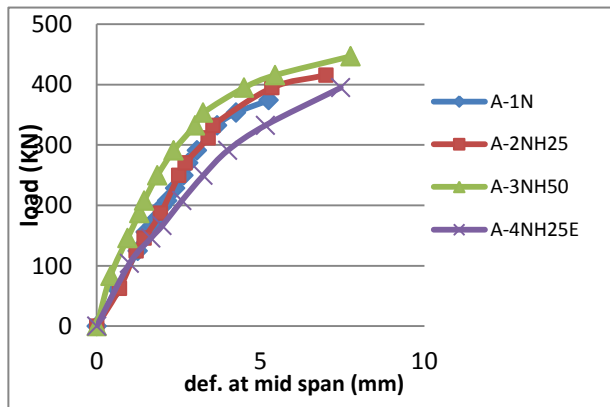


Figure (4): Load – Deflection Cures for Groups A, B.

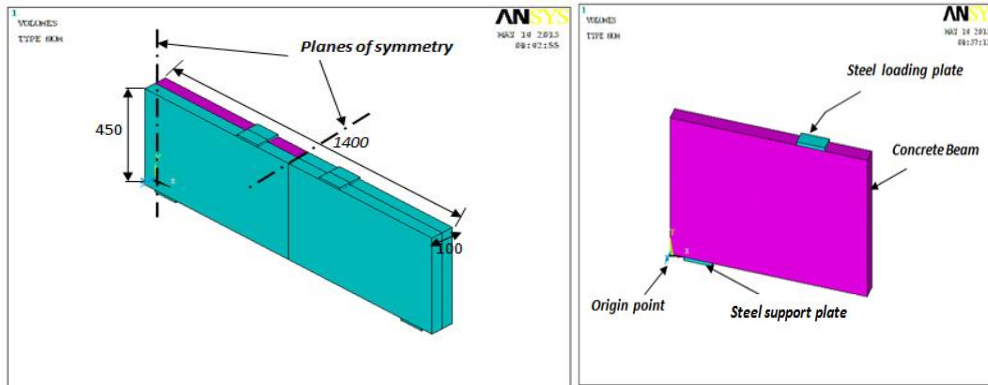


Figure (5): Adopted Quarter of the Deep Beam.

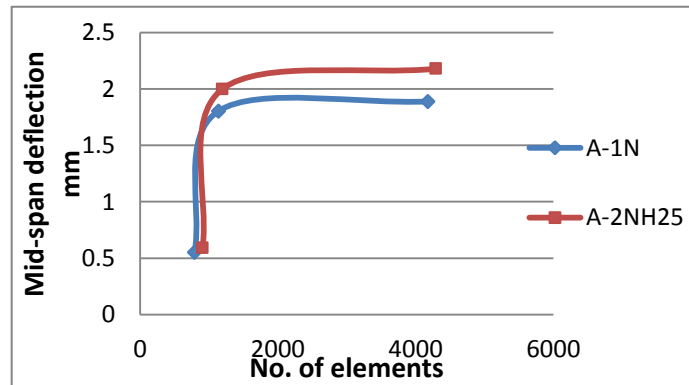


Figure (6): Results of Convergence Study.

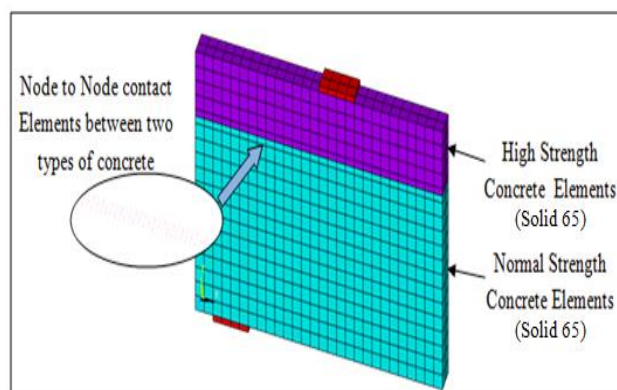
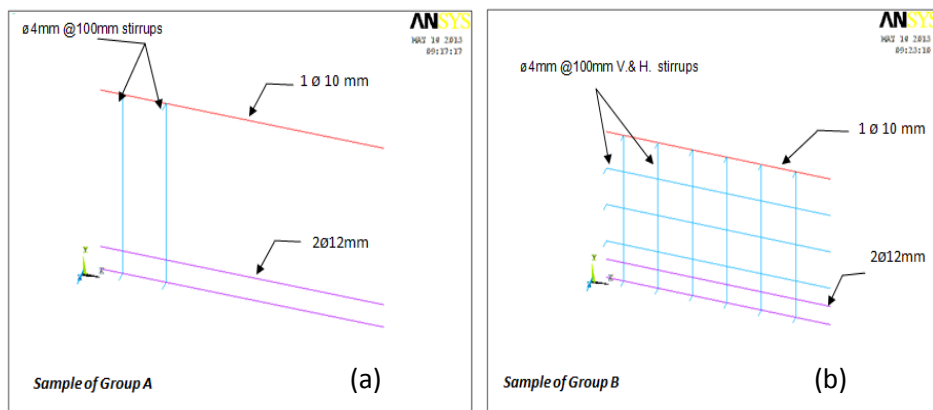
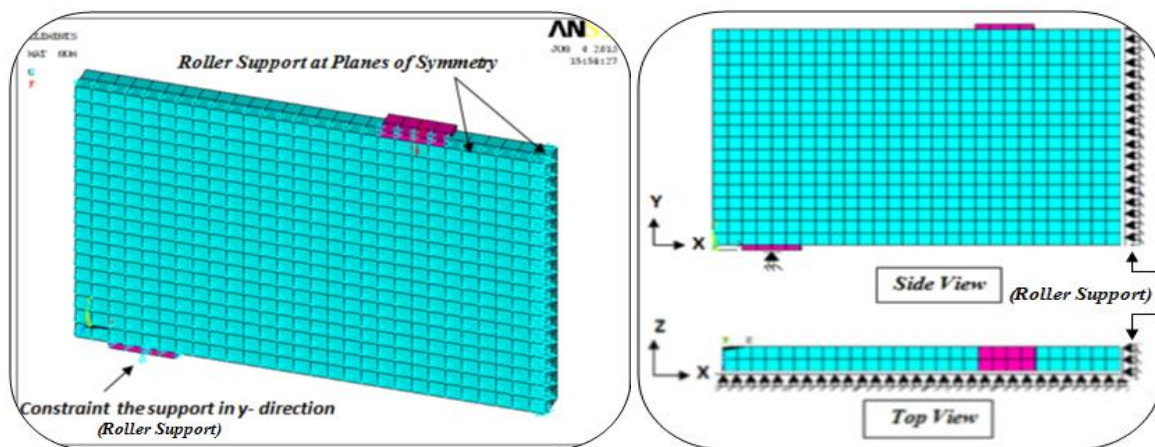


Figure (7): Mesh of the Concrete, Steel Plate, and Steel Support for the Hybrid Beam.



**Figure (8):** Details of Reinforcing Steel Bars: (a) Group A, (b) Group B.



**Figure (9):** Details of Boundary Conditions (Symmetry and Supports) for the Quarter of the Control Beam

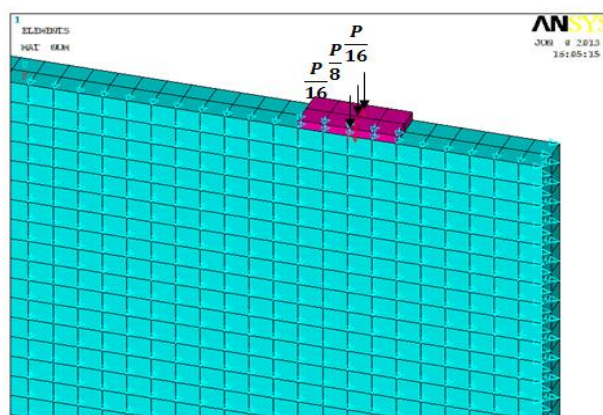


**Figure (10):** Details of the Applied Load at the Loading Plate.

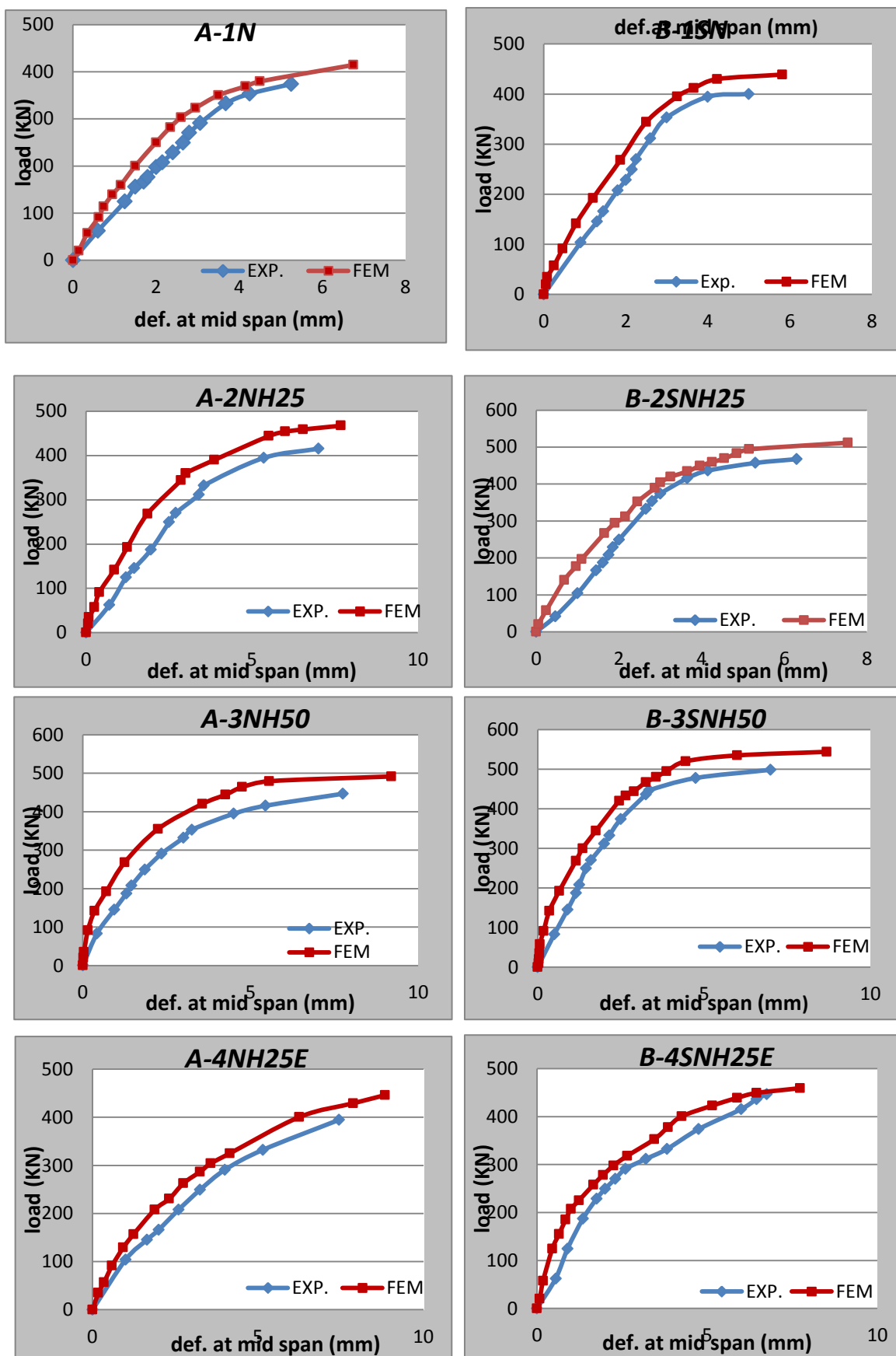
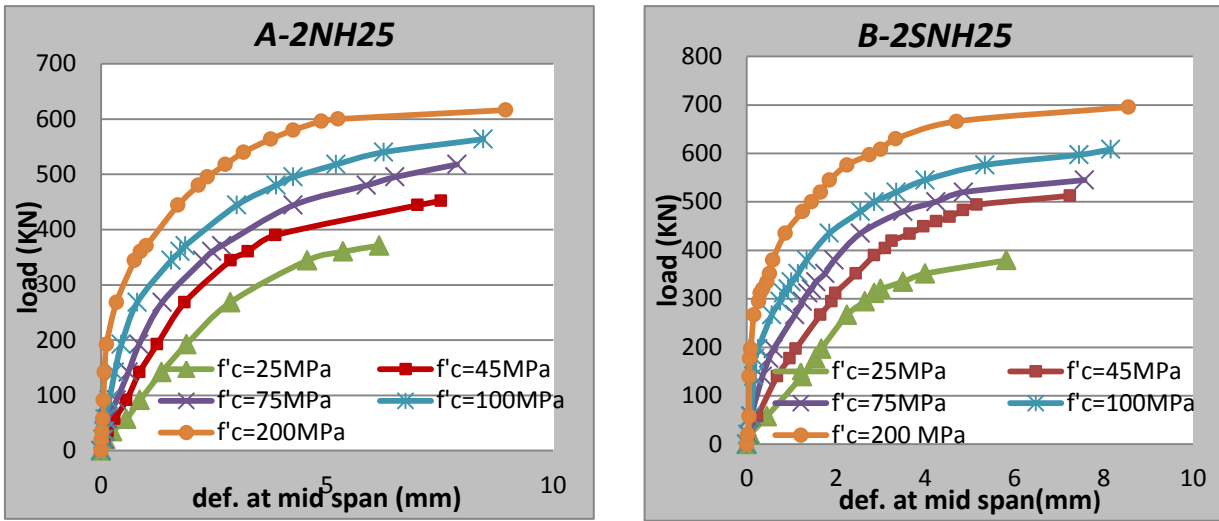
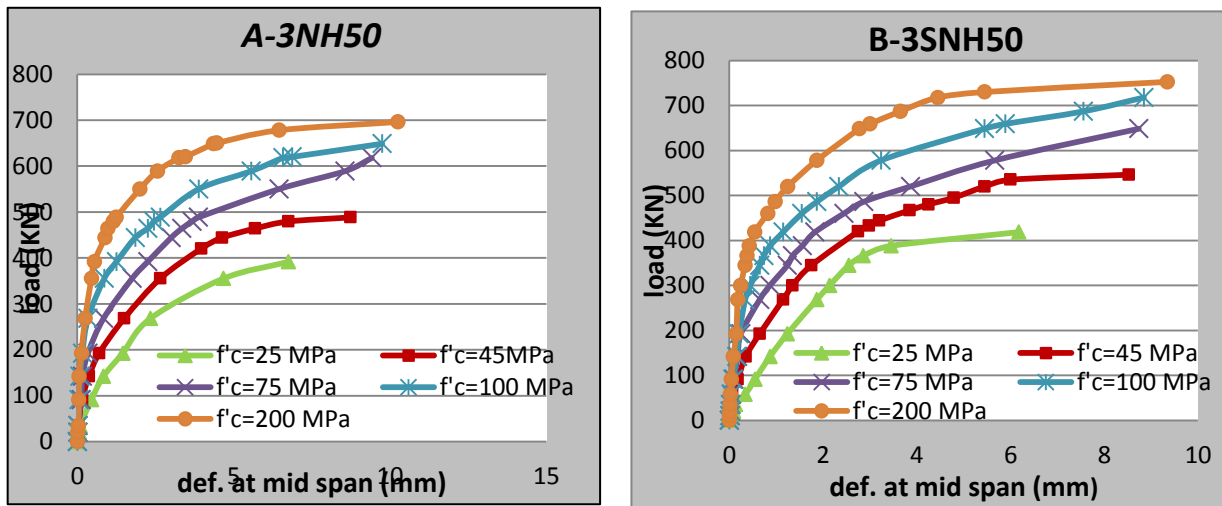


**Figure (11):** Load-Deflection Curve for the Two Groups; A, B



(a)



(b)

Figure (12): Load- Deflection Curves for Hybrid Beams; (a) 25% of total depth (HSC), (b) 50% of total depth (HSC)

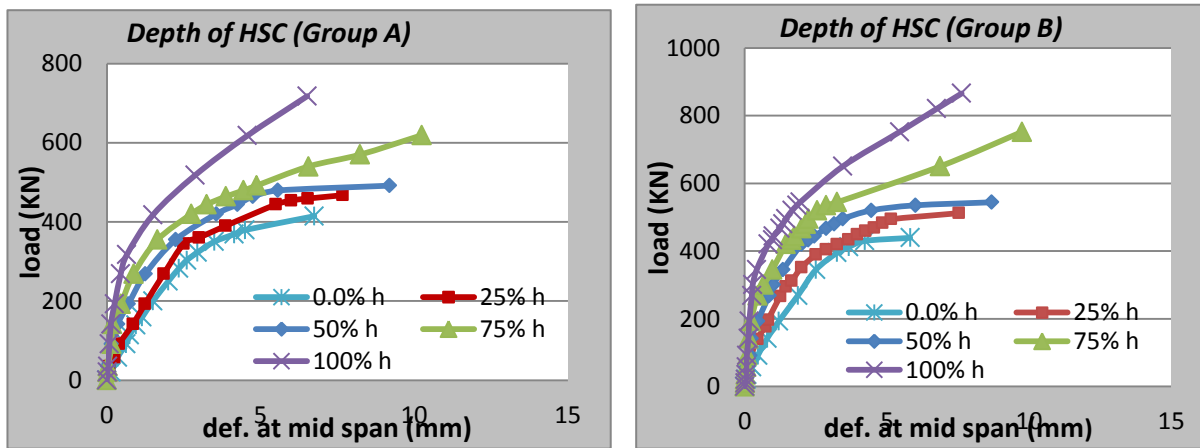


Figure (13): Load- Deflection Curves for the Tested Two Groups (A&B)

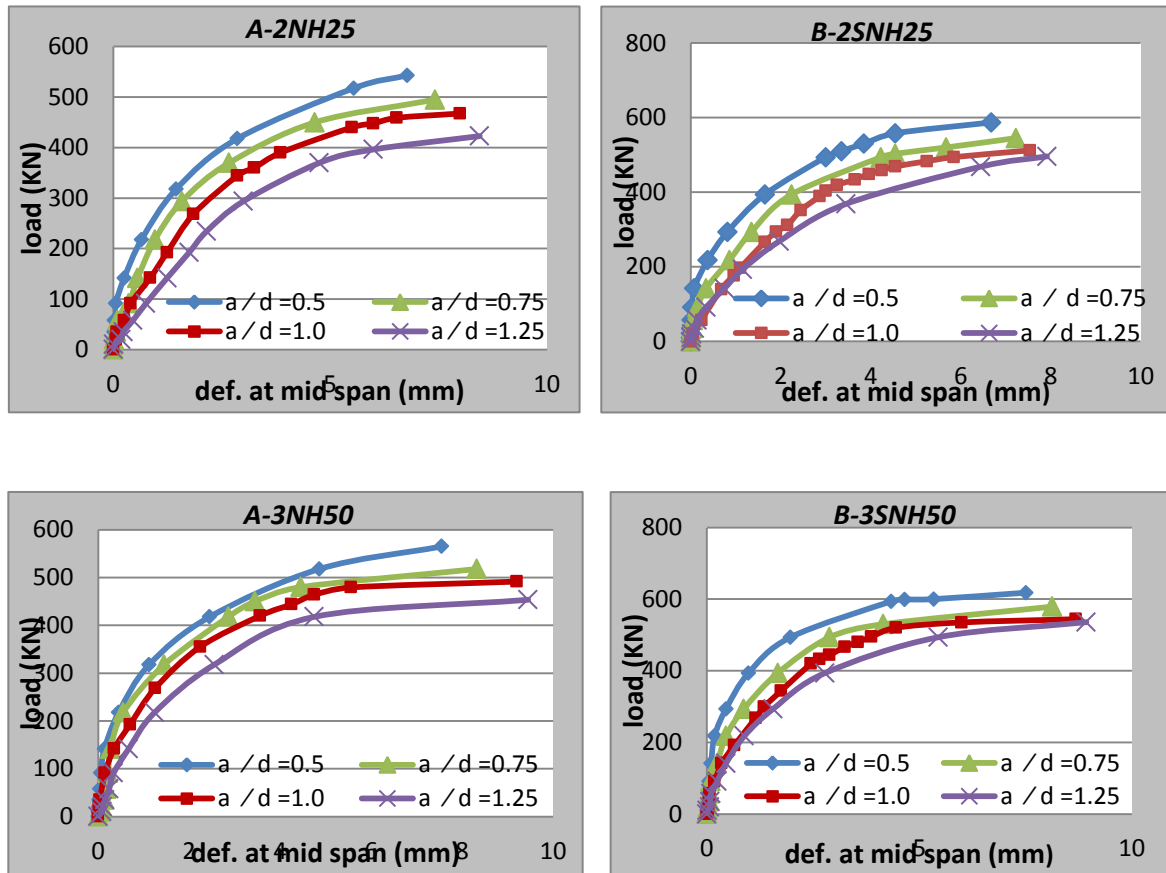


Figure (14): Load- Deflection Curves for Hybrid Beams.

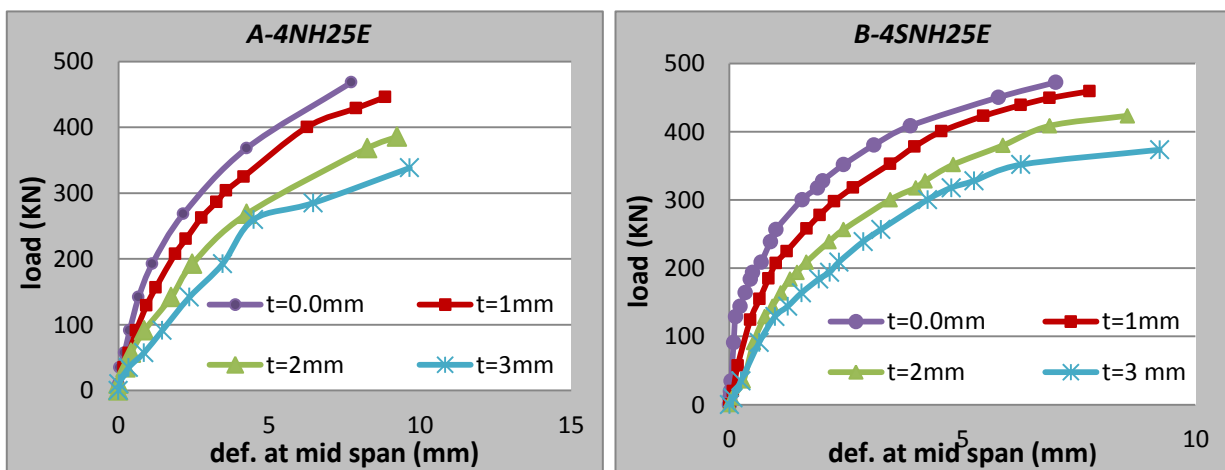


Figure (15): Load- Deflection Curves for Hybrid Beams.